Chapter 6

A Kinetic Model for Stress Fiber Contraction and Relaxation

6.1 Abstract

High-resolution measurement of the force generated by a single fibroblast cell during perturbation with Cytochalasin D (CD) or recovery reveals that the force is quantized. The origin of the force is thought to be a ventral stress fiber in the fibroblast. The magnitude of the quantized jumps in the force (~1 nN) appears to be consistent with a model where individual sarcomeres abruptly assemble or disassemble. Here we consider the dynamics of this process: the measured temporal profile for stress fiber contraction and relaxation and the duration of the force steps. We show that the observed dynamics are consistent with a simple stochastic model in which the time it takes for an individual sarcomere to abruptly assemble or disassemble is exponentially distributed with some characteristic constant rate $1/\tau$. The model is based on three parameters: the number of sarcomeres in the stress fiber N_S, the force step size f_0, and the above timescale τ. The stochastic model makes the following predictions: (1) the total force generated by a stress fiber should follow on average an exponential temporal profile, (2) the length of time between two subsequent force steps should be on average inversely proportional to the number of remaining sarcomeres (yet to assemble/disassemble) and therefore increases with time. The above three parameters (N_S, τ, f_0) were estimated for each measured

profile. Model predictions appear to be in good quantitative agreement with the fibroblast dataset and transition times were found to be statistically consistent with an exponential distribution (applying the Pearson's chi-square test statistic). These findings support the proposed interpretation that sarcomeres assemble abruptly upon polymerization and disassemble abruptly upon depolymerization of actomyosin complexes.

6.2 Introduction

Actin filaments in association with myosin filaments form contractile structures in both muscle and non-muscle cells. One type of actin filament structure found in many types of non-muscle cells involved in adhesion, motility, and morphogenesis, are known as contractile actin stress fibers (*1*-*2*). Structurally, stress fibers are bundles of actin filaments containing bipolar periodic arrays of myosin II between consecutive α-actinin-foci (*1*) (a schematic diagram of a stress fiber is shown in Fig. 6.1). Stress fibers are thus structurally similar to muscle myofibrils and can also similarly produce contractile force, however unlike myofibrils, these structures are less organized (*1*). Furthermore, despite the similarity to myofibrils, stress fibers typically do not display repeatable contraction and relaxation on relatively short time scales but rather contract continuously with occasional relaxing or stretching (*1*).

There are three types of stress fiber that are known to exist: dorsal stress fibers, ventral stress fibers, and transverse arcs (*1*-*2*). Dorsal stress fibers, which typically attach to focal adhesions only at one end, are known to display uniform polarity and therefore may not be contractile structures at all (*2*). Indeed, these structures have never been observed to contract (*1*). Transverse arcs are curved acto-myosin bundles that do not directly attach to focal adhesions. Since these structures are not anchored to the plasma membrane, it is unclear if they can transmit force (*2*), although this may perhaps be achieved indirectly, as these fibers are often observed to interact with dorsal stress fibers, which in turn anchor them to the substrate (*1*). Finally the most commonly observed type of stress fibers are ventral stress fibers. These contractile structures are tethered at both ends to

focal adhesions and are thus capable of generating tension under constant length (*1-2*). Indeed, the majority of the contractile force that a fibroblast applies to the substrate is aligned with the direction of ventral stress fibers (*2*). Thus ventral stress fibers may be the most effective generators of contractile force in these cell types. These type of stress fibers are thought to be responsible for tail retraction as well as other cell shape changes occurring due to increased contraction (*1*). In addition these fibers are thought to work against membrane tension at cell borders (*1*).

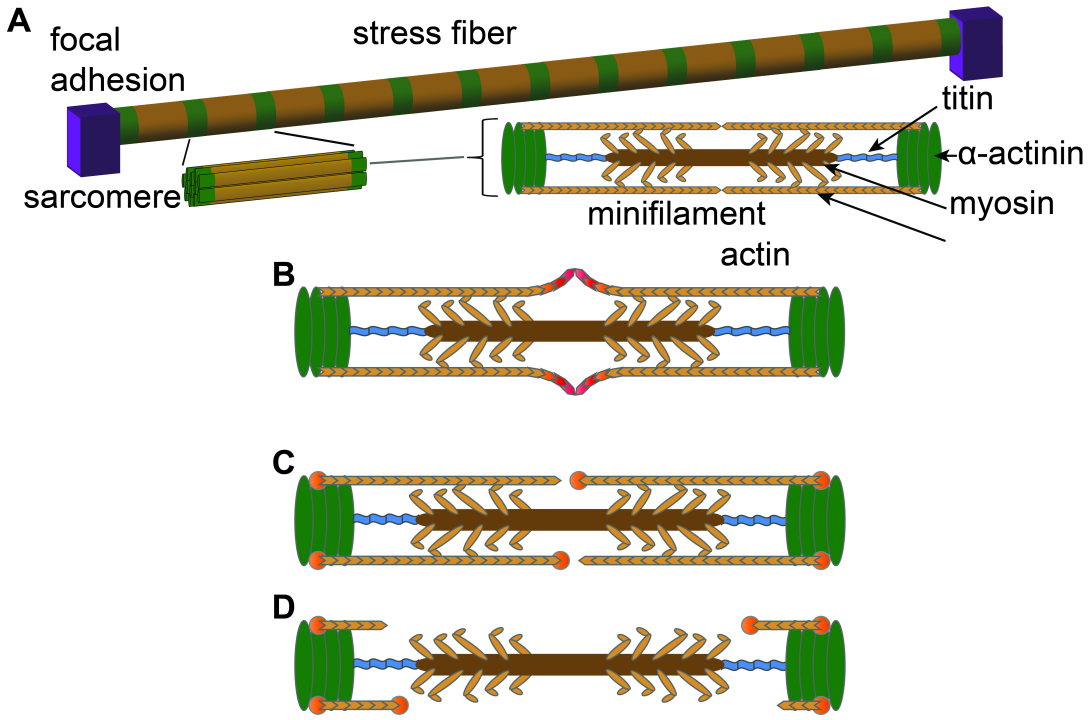

Figure 6.1. Cartoon model of a ventral stress fiber. A. Each stress fiber is thought to be composed of a serial sequence of sarcomeres where each sarcomere is composed of approximately 50 minifilaments in parallel, and each minifilament is composed of a bipolar myosin filament and opposing actin filaments held together by α-actinin and titin. **B.** Cartoon of unperturbed (closed) minifilament, actin polymerization pressure is highlighted in red. In the proposed model we assume that each closed sarcomere generates a discrete unit of force f_0. **C.** Cartoon of minifilament after initial exposure to CD (orange) has stopped actin polymerization. **D.** Cartoon of "open" minifilament after actomyosin complexes have disassembled due to CD exposure. Figure courtesy of Blake Axelrod (Roukes lab, Caltech).

Here we analyze data collected by Blake Axelrod at Caltech, a member of the Roukes group, who measured with the highest resolution to date the force as a function of time of a single fibroblast cell. For this purpose, Blake constructed an instrument that utilizes a polymer Nano-Electro-Mechanical Systems (NEMS) force sensor with integrated piezoresistive strain sensing to measure the force generated by adherent cells (see experimental setup in Fig. 6.2). To precisely control the aqueous media surrounding the cell, the NEMS chips are encapsulated in multi-layer PDMS microfluidics with pneumatically actuated valves. This device allows the experimenter to change the growth medium of cell while it is attached to the force sensor.

In the actual experiment, a single NIH-3T3 fibroblast cell attached itself to a platform adjacent to the force sensor, making contact with the force sensor. An image of this cell in contact with the NEMS device is shown in Fig. 6.3. While in the recovery medium, the calibrated force sensor registered a force of about 20 nN (see force profile in Fig. 6.3). To perturb the cell, Cytochalasin D (CD) was flowed in. CD forms stronger bonds to the barbed ends of the actin filaments than to the pointed ends (*3-4*) leading to depolymerization of the actin filaments, disassembly of the actomyosin complex, and loss of contraction. CD belongs to a class of substances called cytochalasins, that are fast-acting and reversible disruptors of contractile force that have been used extensively over the past 40 years to study the role of actin and contractile forces in various cellular processes (*5*). Despite extensive use and study, how the known molecular mechanisms of CD cause the reversible disruption of stress fiber force generation without dismantling stress fibers remains unclear. Upon exposure to CD, Blake indeed observed a decrease in

force, following an exponential-like profile (Fig. 6.3). Indeed when flowing the recovery medium the force was generated again, presumably owing to repolymerization of the actomyosin complex. This process was repeated for several iterations (Fig. 6.8).

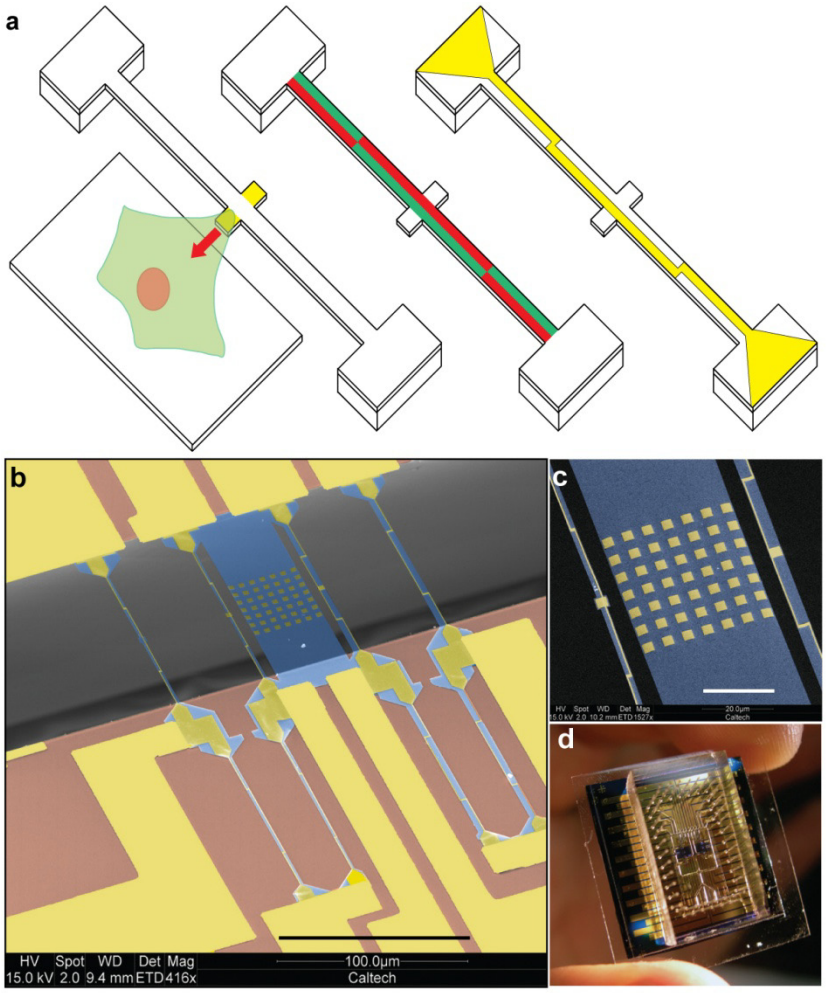

Figure 6.2. NEMS force sensor. a) At left, diagram of the cell on the platform adjacent to the force sensor, cell is spread and attached to the sensor which is coated with fibronectin. At center, contraction generates tensile (green) and compressive (red) strains in the beam. At right, the piezoresistor (yellow) is patterned across the beam to couple only to the tensile strains. **b)** Colorized SEM image of two force sensors, the left one is 2 µm wide, the right is 4 µm wide, both are 100 µm long. The stable platform for the cell is between them. Scale bar is 100 µm. **c)** Colorized SEM image showing close up of two force sensors and platform, gold surface pads and the gold piezoresistors are visible in yellow. Scale bar is 20 µm. **d)** Microfluidics encapsulated chip held between thumb and forefinger. Figure and caption courtesy of Blake Axelrod (Roukes lab, Caltech).

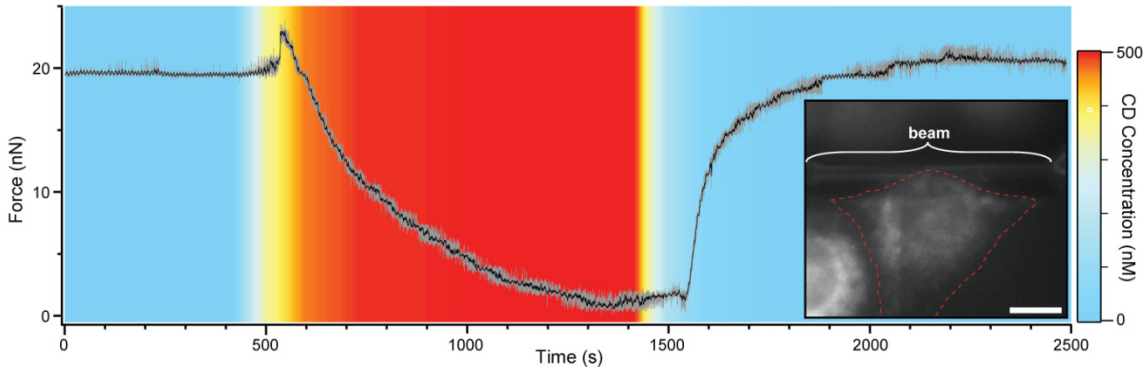

Figure 6.3. Force time time response to CD perturbation. Typical force response to 500 nM CD: switch from conditioned media to CD at 400 sec results in initial contraction. Following the initial contraction, the force drops as expected. At 1400 sec the flow is switched back to conditioned media and the cell re-establishes normal contractile force. The black line is a 1 sec running average, the grey line is the raw data (100 ms integration time, ~200 pN force noise). The background color depicts the CD concentration as estimated using finite elements simulations (COMSOL). There is transit time for the CD solution to reach the cell through the microfluidics after actuating the microfluidic valves at 400 sec and the ~1 nL/sec flow rate takes additional time to displace the conditioned media from the 150 nL chamber. Inset shows fluorescent image of the cell attached to the beam taken immediately before data acquisition, scale bar is 10 μm. Figure and caption courtesy of Blake Axelrod (Roukes lab, Caltech).

When examining the temporal profiles closely, these profiles revealed quantized steps in force during both CD induced relaxation and the post-CD contraction. A close up of the force profiles is shown in Fig. 6.4. When a step-fitting algorithm was applied (*6*), a histogram of the computed step sizes revealed that these steps were remarkably uniform with average step size 1.08 nN ± 0.18 nN (N=96, S.D.). In the following chapter we present our analysis of Blake's experimental data and present a stochastic kinetic model for stress fiber assembly and disassembly that is capable of accounting for the observed temporal dynamics.

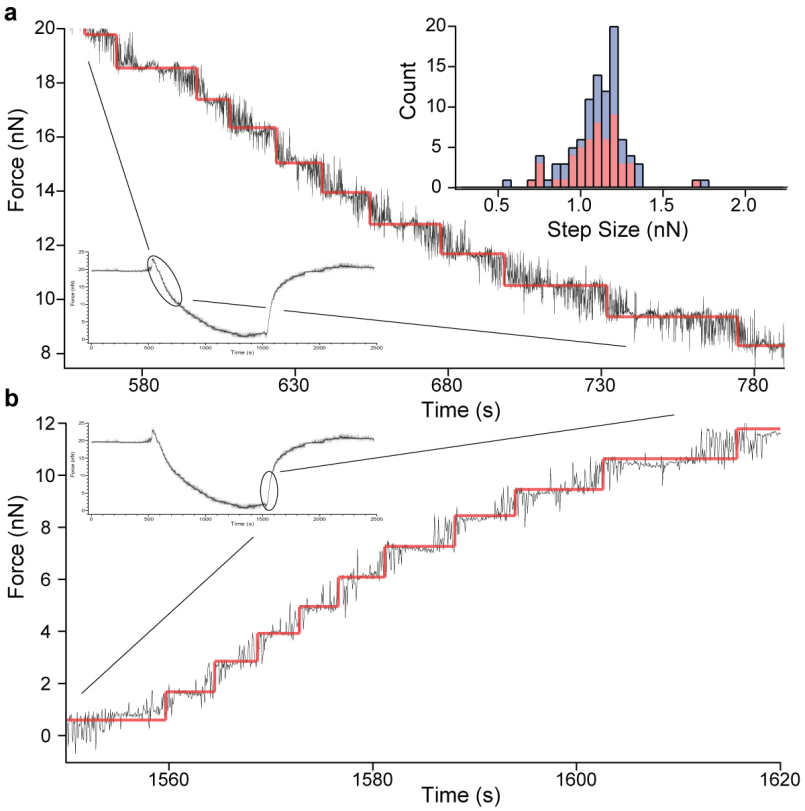

Figure 6.4. Close up of force steps. a) Steps during CD induced force collapse, red is output from step fitting algorithm. Inset is step size histogram for 3 force collapse and recovery cycles. The average step size is 1.08 nN ± 0.18 nN (N=96, error is standard deviation). **b)** Steps during force recovery following return to conditioned media, red is output from step fitting algorithm. Figure and caption courtesy of Blake Axelrod (Roukes lab, Caltech).

6.3 Model development

We assume that each stress fiber is composed of N_S sarcomeres, with each individual sarcomere capable of generating a unit of force f_0, as depicted in Fig. 6.1. The fact that the total force changes in quantized steps suggests that generation of a unit of force by a sarcomere can be approximated by an all-or-none event. Assuming that the quantized steps reflect dynamics of individual sarcomeres it follows that the assembly or

disassembly (i.e., failure) of an individual sarcomere is an all-or-none event with amplitude f_0. Our model is based on the following assumptions: (1) Each sarcomere assembles or disassembles abruptly and irreversibly (i.e., the rate for the reverse reaction to occur is negligible). (2) Sarcomeres assemble or disassemble independently of each other. (3) The time until a sarcomere assembles or disassembles is exponentially distributed (reflecting a certain constant probability rate for this event to occur). (4) The time constant for assembly is the same for all sarcomeres. Similarly, the time constant for disassembly is the same for all sarcomeres. The model is illustrated for the case of disassembly in Fig. 6.5.

Figure 6.5. Schematic model for stress fiber relaxation

According to our model, we assume that the probability distribution for the time it takes a single sarcomere to assemble or disassemble is given by the exponential distribution

(1) $$f(t) = \lambda e^{-\lambda t}.$$

where (henceforth) $\lambda = \lambda_A = \tau_A^{-1}$ for assembly and $\lambda = \lambda_D = \tau_D^{-1}$ for disassembly. The probability that a single sarcomere will assemble or disassemble in the interval $0<t'<t$ is therefore given by:

$$p(t) = \int_{t'=0}^{t} \lambda e^{-\lambda t'} dt' = 1 - e^{-\lambda t}. \tag{2}$$

Hence the average number of sarcomeres to assemble or dissemble by time t is

$$E\mathbf{n}(t) = N_S p(t) = N_S\left(1 - e^{-\lambda t}\right). \tag{3}$$

where $\mathbf{n}(t)$ is the number of sarcomeres that have assembled by time t $\left(0 \le \mathbf{n}(t) \le N_S\right)$ and where E represents the expectation value. The standard deviation of $\mathbf{n}(t)$ is given by the binomial standard deviation

$$\sqrt{\mathrm{var}\left(\mathbf{n}(t)\right)} = \sqrt{N_S pq} = \sqrt{N_S e^{-\lambda t}\left(1 - e^{-\lambda t}\right)}.$$

Considering the case of assembly first, if one assumes that each sarcomere contributes a unit force of f_0 to the total force generated by the stress fiber, then the stochastic force as a function of time would be given by

$$\mathbf{F_{SF}}(t) = f_0 \mathbf{n}(t). \tag{4}$$

Taking the expectation value of $\mathbf{F_{SF}}(t)$ and using Eq. 3 we obtain the expressions for the average and standard deviation of the force of a stress fiber as a function of time:

$$E\mathbf{F_{SF}}(t) = f_0 E\mathbf{n}(t) = f_0 N_S\left(1 - e^{-\lambda_A t}\right) = f_{\max}\left(1 - e^{-\lambda_A t}\right) \tag{5}$$

$$\sqrt{\mathrm{var}\,\mathbf{F_{SF}}(t)} = \sqrt{\mathrm{var}\, f_0 \mathbf{n}(t)} = f_0\sqrt{N_S e^{-\lambda t}\left(1 - e^{-\lambda t}\right)}.$$

where $f_{\max} \equiv f_0 N_S$ is the maximum force generated by the stress fiber. Alternatively, the stochastic force can be written as a sum of N_S steps with an amplitude of f_0, where each step occurs at random times denoted by $\boldsymbol{\tau}_s$ (s=1..N_S):

$$\mathbf{F_{SF}}(\mathbf{t}) = \sum_{s=1}^{N_S} f_0 u(t - \quad_s). \tag{6}$$

where $\boldsymbol{\tau}_s \sim \exp(\lambda)$ and $u(t)$ is a step function ($u(t \geq 0) = 1,\ u(t < 0) = 0$). Note that Eq. 5 can be derived directly from Eq. 6 by taking the expectation value of $\mathbf{F_{SF}}(\mathbf{t})$. The proof is as follows: let's rewrite $u(t - \boldsymbol{\tau}_s)$ in the following form:

$$u(t - \boldsymbol{\tau}_s) = \int_{t'=-\infty}^{\infty} d\,'u(t')\,\delta(t - \boldsymbol{\tau}_s - t').$$

Taking the expectation value $u(t - \boldsymbol{\tau}_s)$ we find that

$$Eu(t - \boldsymbol{\tau}_s) = \int_{t'=-\infty}^{\infty} d\,'u(t')\,E\delta(t - \boldsymbol{\tau}_s - t')$$

$$E\delta(t - \boldsymbol{\tau}_s - t') = \int_{\tau_s=-\infty}^{\infty} d\tau_s f_{\boldsymbol{\tau}}(\tau_s)\delta(t - t' - \boldsymbol{\tau}_s) = f_{\boldsymbol{\tau}}(t - t') = \begin{cases} \lambda e^{-\lambda(t-t')} & t - t' \geq 0 \\ 0 & t - t' < 0 \end{cases}$$

where $f_{\boldsymbol{\tau}}(t)$ is the probability density function of $\boldsymbol{\tau}_s$: $f_{\boldsymbol{\tau}}(t \geq 0) = \lambda e^{-\lambda t}$, $f_{\boldsymbol{\tau}}(t < 0) = 0$. Thus the integrand in $Eu(t - \boldsymbol{\tau}_s)$ is nonzero in the range $0 \leq t' \leq t$:

$$Eu(t - \boldsymbol{\tau}_s) = \int_{t'=-\infty}^{\infty} dt' u(t') f_{\tau}(t - t') = \lambda \int_{t'=0}^{t} dt' e^{-\lambda(t-t')} = e^{-\lambda(t-t')}\Big|_{t'=0}^{t} = 1 - e^{-\lambda t}$$

and thus

$$E\mathbf{F_{SF}}(\mathbf{t}) = E\sum_{s=1}^{N_S} f_0 u(t - \boldsymbol{\tau}_s) = f_0 \sum_{s=1}^{N_S} Eu(t - \quad_s) = f_0 \sum_{s=1}^{N_S} \left(1 - e^{-\lambda t}\right) = f_0 N_S \left(1 - e^{-\lambda t}\right) \therefore$$

For sarcomere disassembly we have

$$\mathbf{F_{SF}}(t) = f_{\max} - f_0 \mathbf{n}(t). \tag{7}$$

Taking the expectation value of $\mathbf{F_{SF}}(t)$ and using Eq. 3 we find that

(8) $$E\mathbf{F}_{\mathbf{SF}}(t) = f_{\max} - f_0 E\mathbf{n}(t) = f_{\max} e^{-\lambda_D t}.$$

In Fig. 6.6A we plot the average stochastic force (Eq. 5) for $N_S = 20$ and λ_A=*1/200 sec*$^{-1}$. Fig. 6.6A also shows a simulation of the stochastic force (Eq. 6). To simulate the stochastic force, the assembly times for $N_S = 20$ sarcomeres were drawn from an exponential distribution with λ_A=*1/200 sec*$^{-1}$. From Fig. 6.6A we see that even though the average time until an individual sarcomere to assemble is long (200 sec), multiple independent sarcomeres will generate steps that can be much shorter than 200 sec, on average following the exponential distribution above. Note that the stochastic model predicts that the waiting time between assembly events generally increases with time. This is shown in Fig. 6.6A for the case of assembly and in Fig. 6.6B for the case of disassembly. Such increasing step times are also observed in the experimental data (e.g., Fig. 6.4). This effect will be discussed in more detail in section 6.7. In Fig. 6.6C we compare the model prediction of the expectation value and standard deviation for the stochastic force with a Monte Carlo simulation in which we averaged 1000 numerical time traces of the stochastic force. The figure shows that the Monte Carlo simulation converged precisely to the analytical expression in Eq. 5.

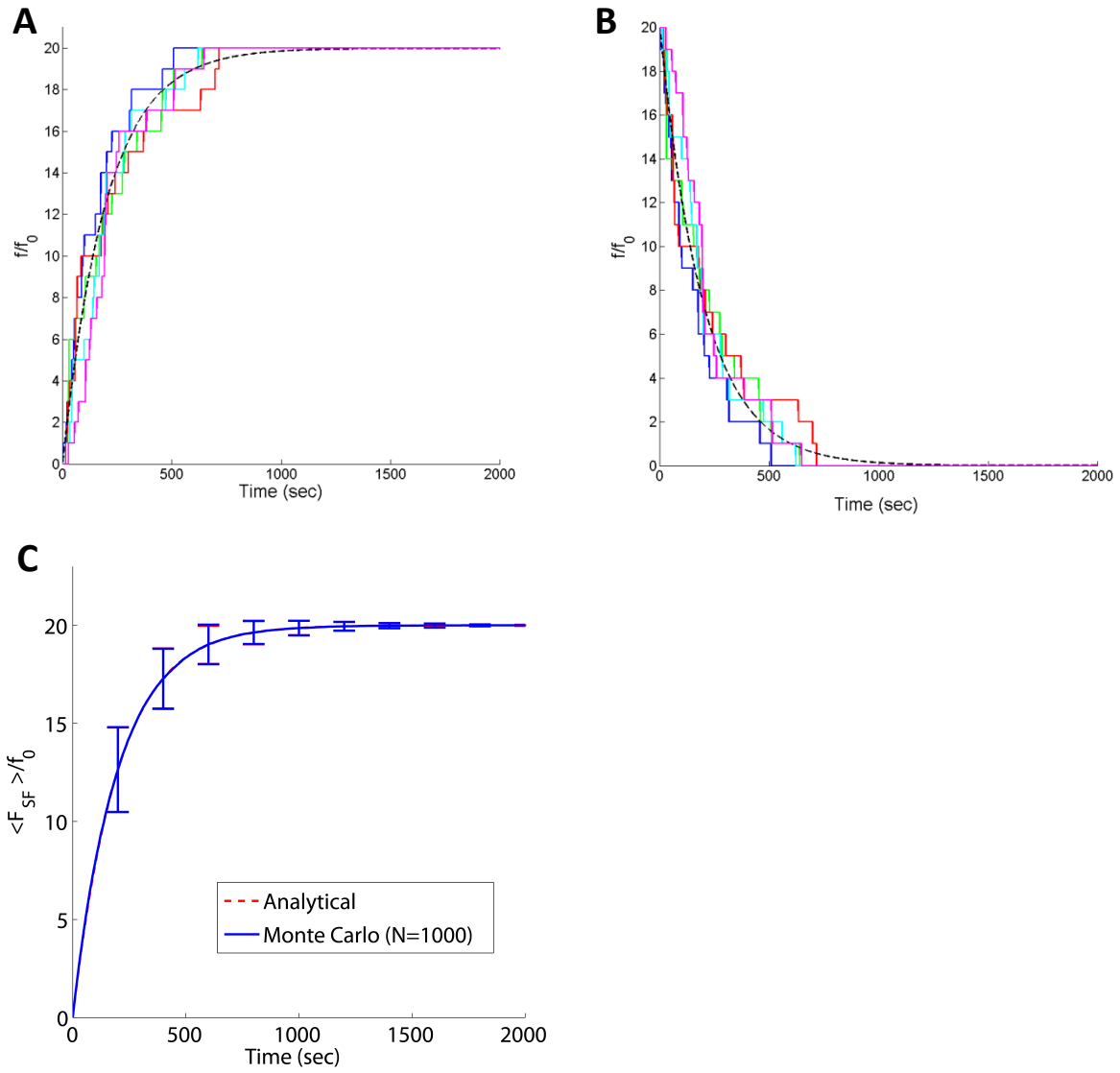

Figure 6.6. Model predictions for stress fiber contraction and relaxation. Analytical predictions are compared with five numerical simulations of stress fiber contraction (**A**) and relaxation (**B**). Each numerical simulation consisted of drawing N_S=20 exponentially distributed variables with rate parameter $\lambda_{A/D}$=1/200 sec^{-1} corresponding to the times that individual sarcomeres assemble (A) or disassemble (B). The analytical predictions for the average force during stress fiber contraction and relaxation are given in Eq. 5 and Eq. 8, respectively. **C.** Monte Carlo simulation of stress fiber contraction, averaging 1000 numerical time traces of the stochastic force (Eq. 6). This ensemble average is compared with the analytical prediction given in Eq. 5. The error bars are standard deviations (both analytical and from the simulation). Analytical predictions and simulation overlap.

6.4 Estimation of stress fiber assembly/disassembly rate

Let t_i be the time for the *i*-th sarcomere to assemble/dissemble (*i*=1..N_S), where *t*=0 is the time of perturbation. We wish to estimate the rate constant $\lambda = \tau^{-1}$. According to our model, $t_i \sim \exp(\lambda)$, therefore $\tau = Et_i$. The maximum likelihood estimator of τ for a given profile is therefore $\hat{\tau} = \frac{1}{N_S}\sum_{i=1}^{N_S} t_i$ (see proof in section 6.10). However, since the exact time of perturbation is not known due to the gradual increase in CD concentration (and there can also be an intrinsic unknown delay in the response of the cell) we cannot estimate the times t_i accurately. Alternatively, if we time order the transition times such that $t_1 < t_2 < \ldots < t_{N_S}$ then it follows that $T_k = t_k - t_m$ for *k*>*m* are independent and exponentially distributed random variables with the same rate λ (see proof in section 6.10). The maximum likelihood estimator of τ for *m*=1 is therefore given by

(9A) $$\hat{\tau}_{ML} = \frac{1}{N_S - 1}\sum_{k=2}^{N_S} T_k .$$

and standard error in the estimation of the mean is given by

(9B) $$S.E. = \sqrt{\mathrm{var}\left(\frac{1}{N_S - 1}\sum_{k=2}^{N_S} T_k\right)} = \frac{\sigma_T}{\sqrt{N_S - 1}} = \frac{\tau}{\sqrt{N_S - 1}}.$$

where for an exponential distribution $\sigma_T = \tau$. A Monte Carlo simulation of Eq. 9 is presented in Fig. 6.12 (section 6.10).

6.5 A statistical test for the distribution of step times

We wish to test the hypothesis that the times $T_k = t_k - t_1$ for a given profile are exponentially distributed with rate $\hat{\lambda} = 1/\hat{\tau}_{ML}$ (estimated for each profile independently). We divide the time axis into three equiprobable regions: [0,0.4τ], (0.4 τ,1.1τ],(1.1τ,∞). The probability for each region is given by:

$$p_1 = \int_0^{0.4\tau} dt\lambda e^{-\lambda t} = 1 - e^{-0.4} = 0.3297$$

$$p_2 = \int_{0.4\tau}^{1.1\tau} dt\lambda e^{-\lambda t} = e^{-0.4} - e^{-1.1} = 0.3374$$

$$p_3 = \int_{1.1\tau}^{\infty} dt\lambda e^{-\lambda t} = e^{-1.1} = 0.3329$$

We then calculate the Pearson's chi-square statistic $X^2 = \sum_{i=1}^{3} \frac{(O_i - E_i)^2}{E_i}$, where O_i and E_i represent the number of observed and expected counts for each bin, respectively, and where for each curve the rate constant was estimated based on Eq. 9. X^2 has a χ^2 distribution with *m-k-1*=3-1-1=1 degrees of freedom, where in this case *m*=3 bins were used and *k*=1 parameters were estimated. Table 6.1 shows the results for three curves, two post-CD contraction events (C1, C2), and one C- induced relaxation (R1)[1]. We see that the *p*-values are high suggesting that statistically the transition times are consistent with an exponential distribution. Other test statistics such as the likelihood ratio test

[1] The cell was cycled between CD and conditioned media 3 times, producing 3 relaxation curves (labeled R1–3) and 3 contraction curves (labeled C1–3). However, due to experimental errors, the CD concentration on one of the cycles was less by an unknown amount; those two cycles were omitted from all of the kinetic model analysis. The Pearson test requires at least 15 step events, thus the Pearson test could be applied to only 3 of the 4 remaining curves (C1, C2, and R1). Curves C1–C3 and R1, R3 are presented in Fig. 6.10 and Fig. 6.11.

statistic $-2\log\Lambda = 2\sum_{i=1}^{3} O_i \log\left(\frac{O_i}{E_i}\right)$ and the Power divergence test statistic with $\lambda = 2/3 : \frac{9}{5}\sum_{i=1}^{3} O_i\left[\left(\frac{O_i}{E_i}\right)^{\frac{2}{3}} - 1\right]$ (expected to give good results for small sample sizes), yield *p*-values identical to the Pearson *p*-value to within 3% (*7*) .

Table 6.1. The Pearson's chi-square test statistic for the step times T_i given a null hypothesis of an exponential distribution

	Contraction curve C1 (*n*=16) $\hat{\tau}$ =106.53±33.91 S.E.		**Contraction curve C2** (*n*=18) $\hat{\tau}$ =77.47 ±16.73 S.E.		**Relaxation curve R1** (*n*=18) $\hat{\tau}$ =231.15±44.94 S.E.	
Interval	**Observed**	**Expected**	**Observed**	**Expected**	**Observed**	**Expected**
[0,0.4τ]	7	5.27	5	5.93	5	5.93
(0.4 τ,1.1τ]	4	5.4	8	6.07	6	6.07
(1.1τ,∞)	5	5.33	5	5.99	7	5.99
X^2	0.947		0.922		0.318	
p-value	0.331		0.337		0.573	

6.6 Comparing the stochastic model to experimental data

Here we compare the measured force traces C1, C2 and R1, R3 with the stochastic model predictions. For each of these four profiles, τ, f_0, and N_S were estimated and the average force was calculated based on Eq. 5 or Eq. 8 depending on the scenario. In Fig. 6.7 we plot the measured force traces and compare them with the profiles predicted by the model. Note that N_S was allowed to change from profile to profile since the number of disassembled or assembled sarcomeres at the beginning of the perturbation is uncertain, and in some cases (curve R3) the profile is given from the middle. Fig. 6.7 shows that the measured traces follow the predicted ensemble averages and are contained within two

standard deviations. Note that the model predicts that any single trace of the force is not exponential (e.g., Fig. 6.6), however the ensemble average of many traces does follow an exponential profile. For this reason deviations between the measured force traces and the predicted ensemble average are expected. In Fig. 6.8 we collapse the transition times for all contraction (or relaxation curves) by scaling the time axis $t \to t/\tau$ and scaling the force axis $F \to F/f_{\max}$. Both contraction curves and both relaxation curves appear to collapse to the same corresponding profiles, as predicted by the model.

6.7 Analysis of step durations

We wish to find the waiting time for the *n*-th sarcomere to assemble (or disassemble) given that *n*-1 sarcomeres have already assembled (or disassembled). For concreteness we will examine the case of assembly. The case for disassembly is analogous. After *n*-1 sarcomeres have assembled, there are $N_S - n + 1$ sarcomeres remaining to assemble. The next event will therefore occur after a time $\mathbf{\Delta t_n}$, which is the minimum time of N_S-n+*1* i.i.d. exponential variables. Since it is known that the minimum of *N* i.i.d. exponentially distributed random variables with rate λ is also exponentially distributed with rate *N*λ, then the time the next event will occur, $\mathbf{\Delta t_n}$, will be exponentially distributed with a rate $\lambda(N_S - n + 1)$. Intuitively, the larger the pool of remaining assembled sarcomeres, the less time one needs to wait until one of the sarcomeres from this pool will fail. Thus initially, when the pool of remaining assembled sarcomeres is large, steps occur in rapid succession, and, with time, as the pool of assembled sarcomeres diminishes, steps also increase in duration.

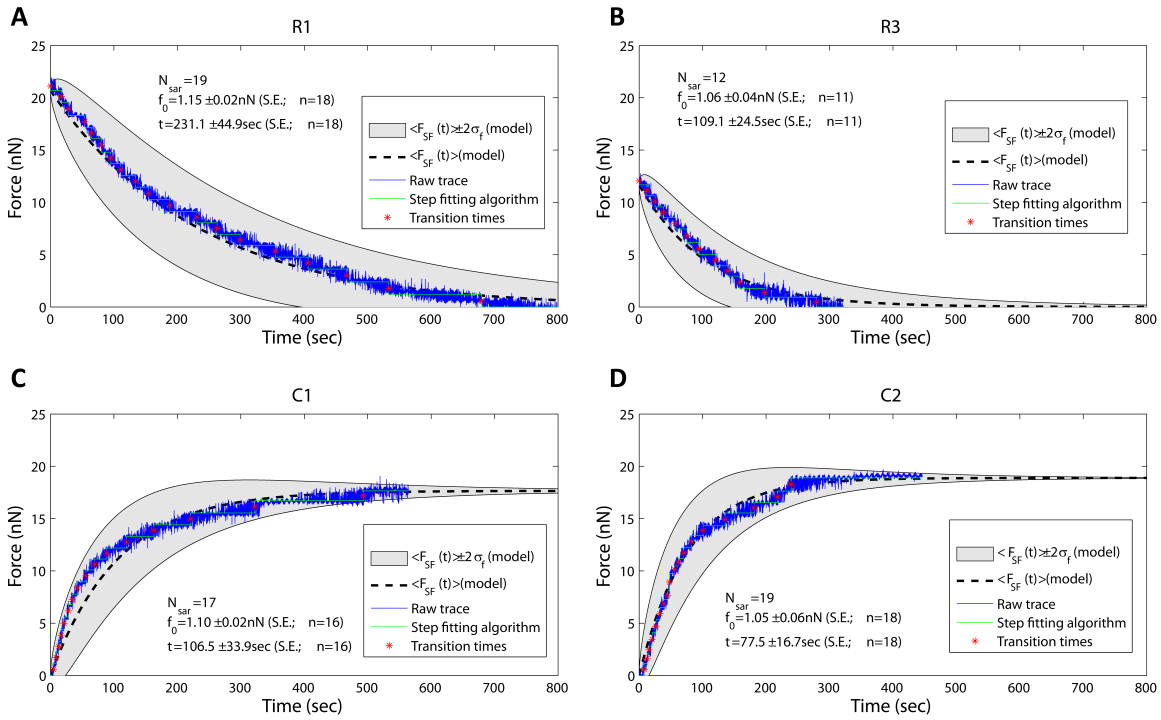

Figure 6.7. Force/time relations predicted by the stochastic model versus experimental data. Model predictions for the average force versus time measurement of a fibroblast perturbed by CD (Eq. 8) (**A** & **B**) or incubated in the recovery medium (Eq. 5) (**C** & **D**). Data is blue, output from step fitting algorithm is red, the discrete step events used to count N_S and calculate f_0 and τ for the kinetic model are yellow. For each profile, τ was estimated based on Eq. 9, f_0 was estimated by averaging the step size of the force predicted by the step fitting algorithm and the number of sarcomeres, N_{sar}, was estimated by the step fitting algorithm as the number of detected steps (note that since the origin was set at the first transition, $N_S = N_{sar} - 1$). Based on these three parameters the expected mean of the force versus time was calculated (dashed curve). This theoretical curve represents the average of many individual stochastic profiles. The shaded area represents the area bounded by the mean plus and minus two standard deviations. C1 and C2 are two contraction profiles with well defined initial conditions and R1 and R3 are two relaxation profiles with well defined initial conditions (see section 6.9).

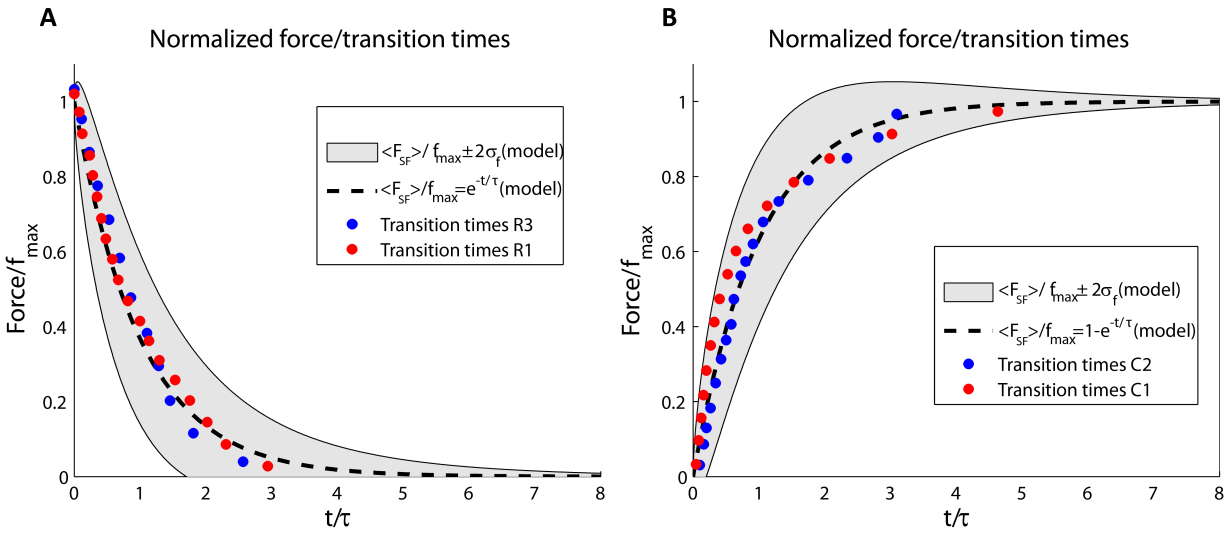

Figure 6.8. Rescaled force/time traces for contraction and relaxation profiles. Force versus step times for contraction (**A**) and relaxation (**B**) scenarios were collapsed by scaling the time axis $t \rightarrow t/\tau$ and the force axis $F \rightarrow F / f_{\max}$ (where $f_{\max} = f_0 N_S$) for each profile. For Methods see caption of Fig. 6.7. The shaded area represents area bounded by the mean plus and minus two standard deviations assuming N_S=18 (giving a lower bound on deviations).

Another way to see this is the following: the probability that a single sarcomere will assemble in the next t seconds is (see Eq. 2) $p(0<t'<t)=1-e^{-\lambda_A t}$. The probability that it will not assemble is therefore $1-p(0<t'<t)=e^{-\lambda_A t}$. The probability that none of the remaining N_S-n+1 sarcomeres assemble during the interval $0<t'<t$ is $\left(e^{-\lambda_A t}\right)^{N_S-n+1}$. Therefore the probability that at least one sarcomere will assemble during the interval $0<t'<t$ is $F(t)=1-e^{-\lambda_A t(N_S-n+1)}$. Hence the probability density function for the time to wait until at least one sarcomere assembles after n-1 sarcomeres have already assembled is $F'(t)=\lambda_A\left(N_S-n+1\right)e^{-\lambda_A(N_S-n+1)t}$, or $\mathbf{\Delta t_n} \sim \exp\left(\lambda_A\left(N_S-n+1\right)\right)$.

The average waiting time for the n-th sarcomere to assemble/disassemble given that n-1 sarcomeres have already assembled (or disassembled) is therefore just the expectation value of an exponential distribution with a rate $\lambda_A(N_S - n + 1)$:

$$E\Delta\mathbf{t}_\mathbf{n} = \left[\lambda\left(N_S - n + 1\right)\right]^{-1}. \tag{10}$$

where n=1..N_S. The standard deviation of $\Delta\mathbf{t}_\mathbf{n}$ is given by the exponential standard deviation: $\sqrt{\mathrm{var}(\Delta\mathbf{t}_\mathbf{n})} = \left[\lambda\left(N_S - n + 1\right)\right]^{-1}$. Note that the inverse of $E\Delta\mathbf{t}_\mathbf{n}$ is linear in n. In Fig. 6.9 we plot Eq. 10, as well as a Monte Carlo simulation for the waiting times. As can be seen from this figure, the numerical simulation converges to the analytically derived expectations value. Standard deviations converge as well (data not shown).

Testing prediction of duration of force steps against experimental data

Waiting times between force steps were estimated for each of the contraction and relaxation experimental curves based on the times extracted by the step-fitting algorithm. In Fig 6.10 we plot the inverse of the experimental waiting times versus the prediction of the stochastic model for these rates (Eq. 10). τ in Eq. 10 was estimated for each profile based on Eq. 9 and N_S was estimated for each profile as the number of steps detected by the step-fitting algorithm. The correlation between the data points and the model prediction was measured by Pearson correlation coefficient to be ρ= 0.72 to 0.95, suggesting that the model predictions were strongly reflected in the data. Note that we

anticipate a high level of noise since the standard deviation equals the predicted rates (see above).

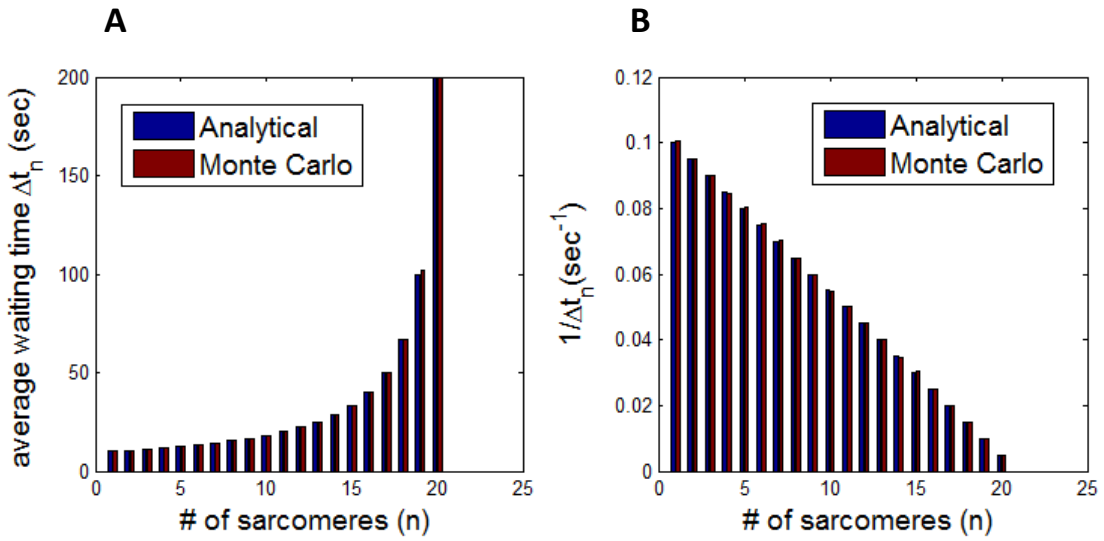

Figure 6.9. Force step durations predicted by the stochastic model compared with a Monte Carlo simulation. A. Each bar represents the average time $E\mathbf{\Delta t_n}$ until the next sarcomere fails, given that n sarcomeres have already failed, thus resulting in n failed sarcomeres. **B.** Predictions for $1/E\mathbf{\Delta t_n}$. Blue bars show analytical predictions based on Eq. 10. Red bars show Monte Carlo simulation results averaging 10^4 repetitions. Each iteration in the Monte Carlo simulation consisted of drawing N_S=20 exponentially distributed times with $\lambda = 1/200$ sec^{-1} and calculating the waiting times between temporally adjacent events. Times were then averaged for all 10^4 iterations.

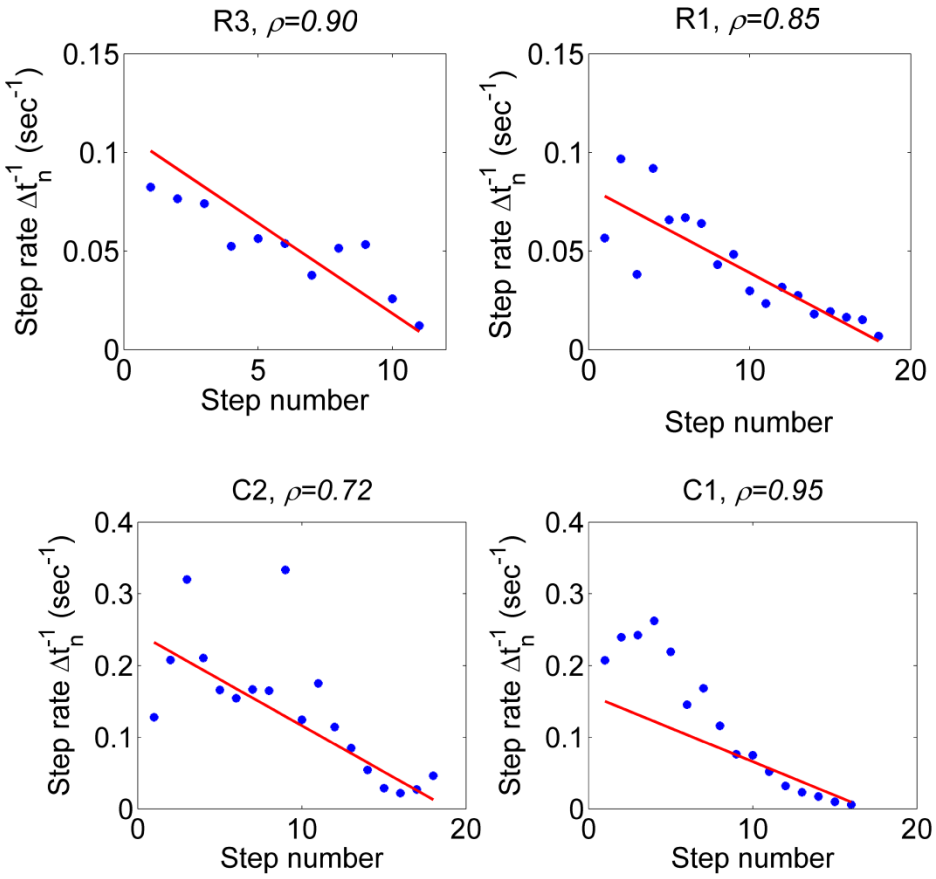

Figure 6.10. Stochastic model prediction of force step durations versus experimental data. The stochastic model prediction for the inverse of the force step durations (red curve) was calculated based on Eq. 10 with τ estimated based on Eq. 9. The experimental data points (blue dots) were calculated as the inverse of the time difference between adjacent steps extracted by the step-fitting algorithm. N_S, the number of observed steps, was determined by the step-fitting algorithm. ρ is the Pearson correlation coefficient measuring the strength of the correlation. C1 and C2 are two contraction profiles with well defined initial conditions and R1 and R3 are two relaxation profiles with well defined initial conditions (see section 6.9).

6.8 Conclusions

We have suggested a simple stochastic model for stress fiber contraction and relaxation that is capable or explaining both qualitatively and quantitatively the response of a single fibroblast cell that was subjected to cyclic perturbation of CD and recovery medium. The model we propose predicts stochastic force/time profiles that are qualitatively similar to the curves observed in the experiment: both predicted and observed curves exhibit an exponential-like profile with step times of increasing length. When rescaled, observed profiles collapse to similar curves that qualitatively follow the ensemble average predicted by the model. Finally, the step onset times are statistically consistent with an exponential distribution and the inverse of the step durations exhibit a high degree of correlation with the linear response predicted by the model. To further substantiate the proposed model it is recommended to repeat this experiment at least one more time, as currently, all data was taken from a single session observing a single cell. An effort to reproduce this data is currently underway.

6.9 Appendix A — Selection criteria of profiles

Figure 6.11 shows the complete measurement of force versus time for the fibroblast cell under investigation, subject to various perturbations. In our analysis we choose to focus on profiles that have the following characteristics: (1) the cell was subject to well-defined perturbations: growth medium (blue) or cytochalasin D (pink), and (2) the initial condition of the cell was well defined, approximating either full contraction or full relaxation of the stress fiber. The profiles that conform to these conditions are: relaxation profiles R3 and R1, which are preceded by contraction profiles C4 and C2, respectively, that leave the stress fibers in a fully contracted condition; contraction profiles C3, C2, and C1, which are preceded by relaxation profiles R3, R2, R1, respectively, that leave the stress fibers in a fully relaxed condition. Profile R2 was not considered for analysis because the CD perturbation was achieved here passively via diffusion, attaining an unknown, yet lower concentration of CD. Profile C3 was rejected due to the back-stepping (this curve is cut short by the step-fitting algorithm, leaving only ~150 sec of data). Since the curve is cut short, estimation of τ using Eq. 9 would be biased. Profile C4 is not considered for analysis because the cell did not appear to respond to the CD perturbation in the preceding period, and therefore the condition of the cell at the onset of C4 was not well defined.

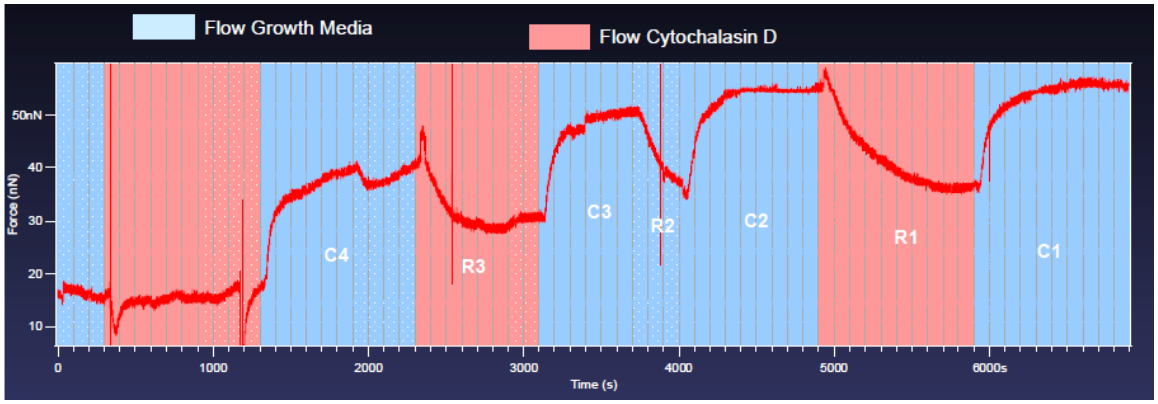

Figure 6.11. Complete force versus time measurement of a single cell. Blue areas represent exposure to growth media, pink areas represent exposure to cytochalasin D, white dots indicate where flow was stopped.

6.10 Appendix B — Time-ordered exponential variables

Lemma 1

Let X_i be N iid exponential random variables (RVs) with rate λ ($1 \le i \le N$). We define

$T_{(1)},...,T_{(m)}$ to be the first m time-ordered RVs (m<N). We wish to show that for $X_i > T_{(m)}$,

$Z_j = X_i - T_{(m)}$ ($j = m+1.. N_S$) are also iid exponential RVs with rate λ, that is

$$f(z_{m+1},...,z_N) = \lambda e^{-\lambda z_{m+1}} \cdot \lambda e^{-\lambda z_{m+2}} \cdot ... \cdot \lambda e^{-\lambda z_N} \quad .$$

Proof:

We define Y_i ($i > m$) to be the N-m RVs that satisfy $X_i > T_{(m)}$

0 $\quad t_{(1)} \quad \ldots \quad t_{(m)} \quad y_{m+1} \quad \ldots \quad y_N$

|----------|----------|----------|----------|-----› .

$\quad dt_{(1)} \quad \ldots \quad dt_{(m)} \quad dy_{m+1} \quad \ldots \quad dy_N$

The joint pdf of $T_{(i)}$ and Y_i is given by

$$P(t_{(1)},...,t_{(m)},y_{m+1},...,y_N) =$$
$$= P\left(one\ \ X_i \in dt_{(1)},...,one\ X_i \in dt_{(m)},one\ X_i \in dy_{m+1},...,one\ X_i \in dy_N\right) =$$
$$= N!\cdot\frac{1}{(N-m)!}\cdot\underbrace{\left(\lambda e^{-\lambda t_{(1)}}dt_{(1)}\cdot...\cdot\lambda e^{-\lambda t_{(m)}}dt_{(m)}\right)}_{m}\cdot\underbrace{\left(\lambda e^{-\lambda y_{m+1}}dy_{m+1}\cdot...\cdot\lambda e^{-\lambda y_N}dy_N\right)}_{N-m}$$

where the normalization factor stems from the fact that there are *N!* ways of ordering *N* variables, however since the Y_i's are not time ordered we need to remove the degeneracy of $(N-m)!$. Thus

$$f(t_{(1)},...,t_{(m)},y_{m+1},...,y_N) = \underbrace{(N-1)\cdot...\cdot(N-m+1)}_{m}\cdot\left(\lambda e^{-\lambda t_{(1)}}\cdot...\cdot\lambda e^{-\lambda t_{(m)}}\right)\cdot\left(\lambda e^{-\lambda y_{m+1}}\cdot...\cdot\lambda e^{-\lambda y_N}\right).$$

Now,

$$f(t_{(1)},...,t_{(m)},y_{m+1},...,y_N) =$$
$$= f(t_{(1)},...,t_{(m)},y_{m+1} = z_{m+1}+t_{(m)},...,y_N = z_N + t_{(m)}) =$$
$$= N\cdot...\cdot(N-m+1)\cdot\left(\lambda e^{-\lambda t_{(1)}}\cdot...\cdot\lambda e^{-\lambda t_{(m)}}\right)\cdot\underbrace{\left(\lambda e^{-\lambda\left(z_{m+1}+t_{(m)}\right)}\cdot...\cdot\lambda e^{-\lambda\left(z_N+t_{(m)}\right)}\right)}_{N-m} =$$
$$= N\cdot...\cdot(N-m+1)\cdot\left(\lambda e^{-\lambda t_{(1)}}\cdot...\cdot\lambda e^{-\lambda t_{(m-1)}}\cdot\lambda e^{-\lambda t_{(m)}(N-m+1)}\right)\cdot\left(\lambda e^{-\lambda z_{m+1}}\cdot...\cdot\lambda e^{-\lambda z_N}\right).$$

Intergrating out $t_{(m)}$:

$$f(t_{(1)},...,t_{(m-1)},z_{m+1},...,z_N) = \int_{t_{(m-1)}}^{\infty} d_{(t_m)}f(t_{(1)},...,t_{(m)},z_{m+1},...,z_N) =$$
$$= N\cdot...\cdot(N-m+1)\cdot\underbrace{\left(\lambda e^{-\lambda t_{(1)}}\cdot...\cdot\lambda e^{-\lambda t_{(m-1)}}\right)}_{m-1}\cdot\left(\lambda e^{-\lambda z_{m+1}}\cdot...\cdot\lambda e^{-\lambda z_N}\right)\cdot\int_{t_{(m)}=t_{(m-1)}}^{\infty}dt_{(m)}\lambda e^{-\lambda t_{(m)}(N-m+1)} =$$
$$= \underbrace{N...\cdot(N-m+2)}_{m-1}\cdot\underbrace{\left(\lambda e^{-\lambda t_{(1)}}\cdot...\cdot\lambda e^{-\lambda t_{(m-1)}(N-m+2)}\right)}_{m-1}\cdot\left(\lambda e^{-\lambda z_{m+1}}\cdot...\cdot\lambda e^{-\lambda z_N}\right).$$

We can now recursively integrate out $t_{(m-1)}$ and so on:

$$f(t_{(1)},...,t_{(m-2)},z_{m+1},...,z_N)=$$

$$=N\cdot...\cdot(N-m+2)\cdot\underbrace{\left(\lambda e^{-\lambda t_{(1)}}\cdot...\cdot\lambda e^{-\lambda t_{(m-2)}}\right)}_{m-2}\cdot\left(\lambda e^{-\lambda z_{m+1}}\cdot...\cdot\lambda e^{-\lambda z_N}\right)\cdot\int_{t_{(m-1)}=t_{(m-2)}}^{\infty}dt_{(m-1)}\lambda e^{-\lambda t_{(m-1)}(N-m+2)}=$$

$$=\underbrace{N\cdot...\cdot(N-m+3)}_{m-2}\cdot\underbrace{\left(\lambda e^{-\lambda t_{(1)}}\cdot...\cdot\lambda e^{-\lambda t_{(m-2)}(N-m+3)}\right)}_{m-2}\cdot\left(\lambda e^{-\lambda z_{m+1}}\cdot...\cdot\lambda e^{-\lambda z_N}\right).$$

Repeating this process *m*-2 more times, (integrating $t_{(1)}$ from 0 to ∞) for $t_{(m-2)}...t_{(1)}$, we obtain $f(z_{m+1},...,z_N)=\lambda e^{-\lambda z_{m+1}}\cdot...\cdot\lambda e^{-\lambda z_N}$ $\therefore$

Simulations supporting theory

In Fig. 6.12 we show the results of a Monte Carlo simulation for the case of *N*=20 and *m*=15, showing that $\{Z_i\}_{i=16..20}$ have properties of an exponential distribution (mean, standard deviation, and probability density function). In Fig. 6.13 we calculate the average "force" step profile and standard deviation of *N*=20 exponential independent RVs when taking into account only the last fifteen RVs measured with respect to the fifth time-ordered RV. This simulation is a precise test of the way in which the experimental data is analyzed. We see that simulations perfectly agree with theory.

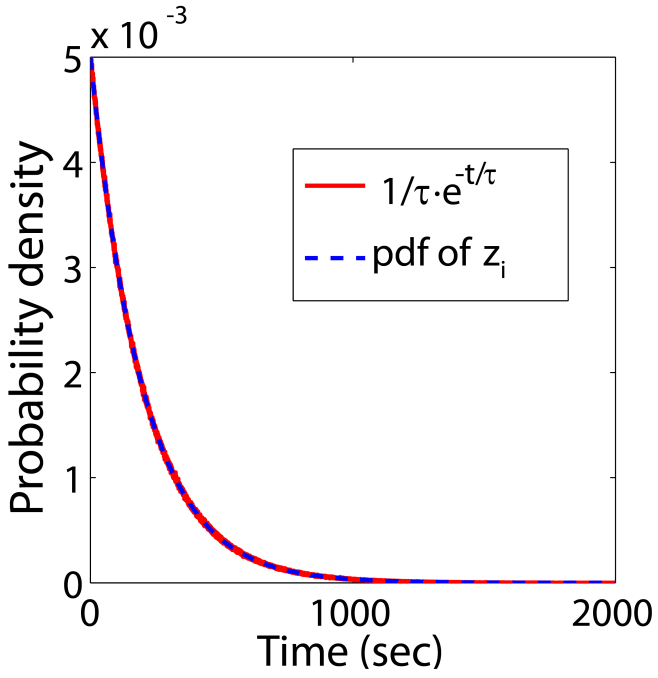

Figure 6.12. Monte Carlo simulation demonstrating lemma 1. This Monte Carlo simulation consisted of 10^7 iterations where in each iteration we drew N=20 exponentially distributed numbers (τ=200 sec) and time ordered them to obtain t_i. We then calculated $z_i = t_i - t_{15}$ for $16 \le i \le 20$ (five RVs in total, corresponding to the case where m=15) and wished to see if z_i indeed behave as i.i.d. exponential RVs with a rate parameter 1/200 sec^{-1} .We therefore calculated the sample mean of z_i for each iteration: $\hat{\mu} = \frac{1}{5}\sum_{i=16}^{20} z_i$ and estimated the mean and standard deviation of $\hat{\mu}$ over all iterations. Based on Eq. 9A and 9B (generalizing these equations to an arbitrary m: $\hat{\tau}_{ML} = \frac{1}{N_S - m}\sum_{k=1+m}^{N_S} T_k, S.E. = \sqrt{\text{var}(\hat{\tau}_{ML})} = \tau / \sqrt{N_S - m}$) we should find that $\hat{\mu}$ converges to τ with a S.E. of $\tau/\sqrt{5}$, i.e.: $E\hat{\mu} = 200 \pm 200/\sqrt{5} = 200 \pm 89.4427$. The simulation yielded 199.98±89.4457 in precise agreement with theory. We also estimated the pdf of z_i by collecting all z_i ($16 \le i \le 20$) and calculating the empirical pdf (red) versus the theoretical pdf (blue). Both curves indeed overlapped.

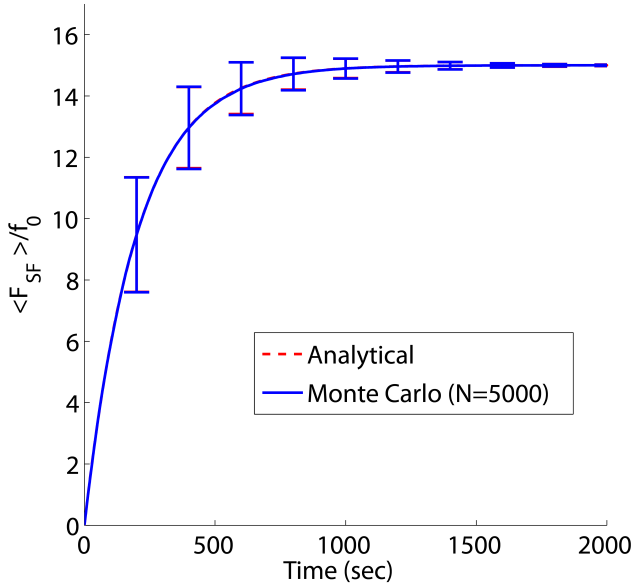

Figure 6.13. Monte Carlo simulation of stress fiber contraction. In each iteration N_S=20 exponentially distributed RVs X_i with λ =1/200 sec^{-1} are drawn. We then time order these 20 RVs, find the fifth time ordered RV, $X_{(5)}$, and form 15 new RVs: $T_j = X_{(j)} - X_{(5)}, j > 5$. Thus T_j represent the times until sarcomeres assemble, measured with respect to the time that the fifth sarcomere assembled (thereby generalizing the case discussed in Fig. 6.6C for $m > 0$). We then construct the stochastic force time trace (Eq. 6), where the step functions occur at times $t = T_j$. Finally we average 5000 of these force traces. We superimpose the theoretical prediction based on Eq. 5 (assuming 15 steps). The error bars are the theoretical and simulated standard deviations. We see that analytical predictions and simulation overlap.

Lemma 2

Let T_i be N i.i.d. exponential RVs with rate λ ($1 \le i \le N$). The ML estimator of $\tau = 1/\lambda$ is

$$\hat{\tau}_{ML} = \frac{1}{N}\sum_{i=1}^{N} t_i \, .$$

Proof:

$$f(t_1, t_2, ..., t_N) = \lambda e^{-\lambda t_1} \cdot \lambda e^{-\lambda t_2} \cdot ... \cdot \lambda e^{-\lambda t_N} = \lambda^N e^{-\lambda (t_1 + ... t_N)}$$

$$\log\left(f(t_1, t_2, ..., t_N)\right) = N \log \lambda - \lambda (t_1 + ... t_N) = -N \log \tau - \frac{1}{\tau}(t_1 + ... t_N)$$

$$\frac{\partial \log\left(f(t_1, t_2, ..., t_N)\right)}{\partial \tau} = \frac{-N}{\tau} + \frac{1}{\tau^2}(t_1 + ... t_N)$$

$$\frac{-N}{\hat{\tau}_{ML}} + \frac{1}{\hat{\tau}_{ML}^{\,2}}(t_1 + ... t_N) = 0$$

$$\hat{\tau}_{ML} = \frac{1}{N}(t_1 + ... t_N)$$

$\therefore$

6.11 References

1. P. Naumanen, P. Lappalainen, P. Hotulainen, *J. Microsc.* **231**, 446 (2008).
2. S. Pellegrin, H. Mellor, *J. Cell Sci.* **120**, 3491 (2007).
3. J. A. Cooper, *Journal of Cell Biology* **105**, 1473 (1987).
4. P. Sampath, T. D. Pollard, *Biochemistry* **30**, 1973 (Feb, 1991).
5. J. R. Peterson, T. J. Mitchison, *Chemistry & Biology* **9**, 1275 (Dec, 2002).
6. J. W. J. Kerssemakers *et al.*, *Nature* **442**, 709 (Aug, 2006).
7. T. R. C. Reed, N. A. C. Cressie, *Goodness-of-Fit Statistics for Discrete Multivariate Data*. Springer, Ed., Springer Series in Statistics (Springer, 1988), p. 211.